Finite-difference multiple fluid solution for source-driven rotation in highly magnetized linear plasma device

T. Rubin,[a] (iD) E. J. Kolmes, (iD) I. E. Ochs, (iD) M. E. Mlodik, (iD) and N. J. Fisch (iD)

AFFILIATIONS

Department of Astrophysical Sciences, Princeton University, Princeton, New Jersey 08544, USA

[a] Author to whom correspondence should be addressed: trubin@princeton.edu

ABSTRACT

The rotation profile of a magnetized plasma cylinder composed of multiple fluids is investigated analytically, expanding on previous results. The analytic steady-state solution is used as a benchmark for a time-dependent multiple-fluid finite-difference code, MITNS: Multiple-Ion Transport Numerical Solver. Magnetic field evolution is taken into account, both analytically and numerically. Its details are shown to be of importance when particles are allowed out of the domain. MITNS reproduces the asymptotic expansion results for a small parameter $\delta \lll 1$. For $\sqrt{m_e/m_i} \sim \delta \lll 1$, a slightly different regime, dominated by viscosity-induced transport of ions, is found numerically and analytically. This verification supports the use of this code for more complex time-dependent calculations in the future. Additionally, we derive the angular velocity profile of each species due to radial particle and charge fluxes of various strengths.

Published under an exclusive license by AIP Publishing. https://doi.org/10.1063/5.0070292

I. INTRODUCTION

A cylindrical plasma geometry is used in fusion applications, such as mirrors,[1,2] z-pinches,[3] MagLIF,[4–7] and in some centrifugal fusion concepts,[8–12] as well as mass separation applications, such as plasma centrifuges.[13–26] Investigation of classical transport effects is a first step in modeling of these devices.

Literature regarding the classical transport in plasma, employing Braginskii[27] transport equations, or equivalent formulations for multi-species multi-fluid plasmas,[28] is extensive, containing predictions for flow profiles,[29] currents,[30] and impurity pinches[11,31] expected in multi-fluid plasmas. The rotation profile in such devices affects the centrifugal force and shear stress, and through them the ion density profiles,[11] and viscous heating.[32] Radial and azimuthal currents depend on the rotation profile as well.[30] Differential rotation of ion species results in ion–ion frictional heating and enhanced heat transport[33] (Ettingshausen effect).

A multiple-fluid model of classical cross field transport involves solving $4N$ partial differential equations, for the densities, momenta and energies for the N fluids. This equation set is complemented by $14N$ boundary conditions ($2N$ particle fluxes, $4N$ momenta fluxes, $2N$ energy fluxes, in addition to $4N$ momenta diffusion terms, and $2N$ heat diffusion terms), in addition to $4N$ possible volumetric source terms, such as particle injection, wave-driven body forces or laser heating. The evolution of such plasma is nonlinear and complex.

Tailoring the rotation profile might result in enhanced device performance, but the number of boundary conditions and source terms requires a numerical tool able to take these terms into account all together.

There are many plasma simulation codes. Some solve the Braginskii single ion and electron fluid,[34] or add neutral species.[35,36] Some solve anomalous transport N-fluid models with a common temperature profile,[37–42] and others solve N-fluid unmagnetized plasma.[43–45]

MITNS: Multiple-Ion Transport Numerical Solver,[46] is just such a numerical tool, solving an arbitrary number of one-dimensional coupled ion-fluid equations—for species specific density, velocity and pressure—in addition to Faraday's law for magnetic field evolution, and the electron pressure equation. Electron density and velocity are taken into account using an MHD-like approximation, which enforces quasi-neutrality to the order of the square of the ratio of Alfvén speed and the speed of light.

In this paper, we extend the slab code MITNS to a cylindrical geometry. This code is used to numerically verify the previous results from Kolmes et al.,[30] discuss the validity of some assumptions present there, and explore a different equation ordering.

Kolmes et al.[30] ordered the momentum equations of ion–electron plasma and categorized three physical mechanisms for cross field radial current in magnetized plasma. Additionally, they derived the leading order angular velocity profile of the plasma from Ohm's law and discussed the possibility of tailoring the rotation profile of the plasma, assuming a temperature profile can be imposed.

This code is capable of evolving not only the ion continuity and momentum equations, and the magnetic field equation, but also the pressure equation for all species. This enables detailed simulations, accounting for the differences in actuation mechanisms (e.g., boundary driven systems vs source driven systems, etc.), and the different resulting regimes (e.g., magnetic field dynamics, heating).

Potential use cases for this code are the time evolution of laser-heated plasma columns, which partition the heat to the electrons more so than the ions, and the tracking of impurities in such scenarios. Or solving for the heat dissipation and pressure buildup of counter-flowing fluxes, as would occur in steady-state fusion devices.

This paper is organized as follows: in Sec. II, we present the model equations. In Sec. III we discuss the previous solution, and add to it the magnetic field equation. In Sec. IV we compare simulation results to a steady-state solution, and in Sec. V we re-derive the angular velocity profile of each species of a multi-species plasma, expanding on Kolmes *et al.*[30] treatment of a two-fluid plasma, by accounting for different magnitudes of radial particle and current fluxes.

II. MULTIPLE FLUID EQUATIONS FOR CYLINDRICAL PLASMA DEVICE

In this section, we present the model equations for an *N*-fluid system with imposed temperature profiles, using the closure by Zhdanov.[28] The treatment is confined to cylindrical coordinates, with gradients only in the radial direction. Using these equations, a leading order solution to the angular velocity profile, density, and magnetic field is derived.

For a fluid plasma composed of several species, the continuity and momentum equations for each species are

$$\frac{\partial n_s}{\partial t} + \nabla \cdot (n_s \mathbf{v}_s) = s_s, \tag{1}$$

$$\frac{\partial}{\partial t}(m_s n_s \mathbf{v}_s) + \nabla \cdot (m_s n_s \mathbf{v}_s \mathbf{v}_s) + \nabla \cdot \pi_s + \nabla p_s$$
$$= Z_s e n_s (\mathbf{E} + \mathbf{v}_s \times \mathbf{B}) + m_s s_s \mathbf{v}_s^{src} + \sum_{s'} (\mathbf{R}_{ss'} + \mathbf{f}_{ss'}). \tag{2}$$

Quantities with a subscript *s* represent a species-dependent quantity, such as n_s, the number density of particles of species *s*. The symbol *t* denotes the time, and **v** denotes the vector fluid velocity. The quantity *s* denotes a particle source, while *m* is the particle mass, π refers to the viscous stress tensor, *p* denotes the pressure, *Z* is the charge number, *e* is the elementary charge, and **E** and **B** are the vector electric and magnetic fields. The term $m s \mathbf{v}^{src}$ represents a momentum source due to injection of particles with initial average (fluid) velocity $\mathbf{v}^{src}$.

The friction body force $\mathbf{R}_{ss'}$ and the thermal friction ("Nernst") body force $\mathbf{f}_{ss'}$ between species *s* and *s'* are expressed as

$$\mathbf{R}_{ss'} = m_s n_s \nu_{ss'} (\mathbf{v}_{s'} - \mathbf{v}_s), \tag{3}$$

$$\mathbf{f}_{ss'} = \frac{3}{2} \frac{m_s n_s \nu_{ss'}}{Z_s Z_{s'} eB} \hat{b} \times \frac{Z_{s'} m_s T_s \nabla T_s - Z_s m_s T_{s'} \nabla T_{s'}}{m_s T_{s'} + m_{s'} T_s}, \tag{4}$$

where $\nu_{ss'}$ is the collision frequency between species *s* and *s'*, *B* is the magnitude of the magnetic field, $\hat{b}$ is a unit vector in the direction of the magnetic field, and *T* is the temperature (in units of energy).

The magnetic field is taken to be in the perpendicular $\hat{z}$ direction. The resultant viscous stress tensor divergence, using the Braginskii[27] and Zhdanov[28] closure, is

$$\nabla \cdot \pi_s = \frac{\partial}{\partial r}\left[\frac{\eta_{s0}}{3r}\frac{\partial}{\partial r}(r v_{sr})\right]\hat{r}$$
$$- \frac{1}{r^2}\frac{\partial}{\partial r}r^3\left[\eta_{s1}\frac{\partial}{\partial r}\left(\frac{v_{sr}}{r}\right) + \eta_{s3}\frac{\partial}{\partial r}\left(\frac{v_{s\theta}}{r}\right)\right]\hat{r}$$
$$- \frac{1}{r^2}\frac{\partial}{\partial r}r^3\left[\eta_{s1}\frac{\partial}{\partial r}\left(\frac{v_{s\theta}}{r}\right) - \eta_{s3}\frac{\partial}{\partial r}\left(\frac{v_{sr}}{r}\right)\right]\hat{\theta}. \tag{5}$$

The coefficients η_{s1} and η_{s3} are expressed as

$$\eta_{s1} = \frac{p_s}{4\Omega_s^2}\sum_{s'}\frac{\sqrt{2}m_s m_{s'}\nu_{ss'}}{(m_s + m_{s'})^2}\left(\frac{6}{5}\frac{m_{s'}}{m_s} + 2 - \frac{4}{5}\frac{\Omega_s}{\Omega_{s'}}\right), \tag{6}$$

$$\eta_{s3} = \frac{p_s}{2\Omega_s}, \tag{7}$$

where Ω_s denotes the signed Larmor frequency for species *s*.

In Cartesian coordinates, the divergence of the viscous stress is a diffusion of linear momentum, $\mathbf{P}_s = m_s n_s \mathbf{v}_s$. The second and third lines in Eq. (5) take the form of a diffusion term for $\mathbf{r} \times \mathbf{P}_s$, the angular momentum, and $\mathbf{r} \cdot \mathbf{P}_s$, the mass flux. Specifically, it is not a diffusion term for $m_s n_s v_{sr}$ and $m_s n_s v_{s\theta}$. More details are discussed in Sec. V.

The magnetic field evolution is determined by Faraday's law,

$$\frac{\partial \mathbf{B}}{\partial t} = -\nabla \times \mathbf{E}. \tag{8}$$

Alternatively, the magnetic field can be determined in steady state from Ampère's law,

$$\nabla \times \mathbf{B} = \mu_0 \mathbf{j}, \tag{9}$$

with **j** being the current density and μ_0 being the permeability of free space.

III. SOURCE-DRIVEN ROTATION

In a recent paper, Kolmes *et al.*[30] ordered the steady-state velocity terms in Eqs. (2) in powers of

$$\delta \doteq \frac{E}{r\Omega_i B}, \tag{10}$$

$$\epsilon \doteq \frac{\nu_{ie}}{\Omega_i}, \tag{11}$$

with respect to the $\mathbf{E} \times \mathbf{B}$ flow velocity, which is taken to be leading order in Braginskii's expansion. In this paper, the symbol "$\doteq$" in used in the meaning of "defined as," for nonstandard expressions. Their solution to the (single) ion and electron fluids was expressed in terms of the ion particle flux,

$$\Gamma_i(r) \doteq r n_i v_{ir} = \Gamma_i(r_i) + \int_{r_i}^r r s_i dr, \tag{12}$$

and the electric charge source,

$$C(r) \doteq r j_r = e\sum_s Z_s \Gamma_s. \tag{13}$$

Here, we use the subscript *i* for the ion fluid, and *e* for the electron fluid. The subscript *p* is used for a reference proton fluid.

One might note that in cylindrical geometry with $\frac{\partial}{\partial t} = \frac{\partial}{\partial z} = \frac{\partial}{\partial \theta} = 0$, electric charge conservation dictates $C \equiv 0$. The case $C \neq 0$ can only be interpreted as a proxy for a charge transport process

outside of the radial classical transport scope of this work, such as a kinetic or wave-driven phenomenon. Alternatively, one can think of it as a proxy for the axial variation, see Appendix A.

Using $\tilde{X}$ to denote a dimensionless quantity corresponding to a physical quantity X, the ordinary differential equations (ODEs) describing the leading order dimensionless rotation $\tilde{\omega}_{rot}$ and density profiles have been derived [Eqs. (28) and (48)] in Ref. 30,

$$\tilde{\omega}_{rot} \doteq -\frac{E}{rB}\frac{R}{v_{thi0}}, \tag{14}$$

$$\tilde{r}^3 \tilde{\eta} \tilde{\omega}'_{rot} = \tilde{r}^2 Q\mathcal{P}\tilde{\Gamma}\tilde{\omega}_{rot} + \mathcal{I}\int_0^{\tilde{r}} \tilde{r}' \tilde{C}\tilde{B}(\tilde{r}')d\tilde{r}', \tag{15}$$

$$\mathcal{P}\tilde{\Gamma} = \tilde{r}\frac{\tilde{n}_i \tilde{n}_e}{\tilde{T}_e^{3/2}\tilde{B}^2}\left[\left(1 + \frac{Z_i m_e}{m_i}\right)\tilde{r}\tilde{\omega}_{rot}^2 - \frac{\tilde{p}'_i + \tilde{p}'_e}{\tilde{n}_i} + \frac{3}{2}Z_i\tilde{T}'_e\right], \tag{16}$$

with Eq. (16) being a correction to Eq. (28) in Ref. 30, in which the $\tilde{r}\tilde{\omega}_{rot}^2$ term is erroneously multiplied by $\tilde{T}_i$. Here, $v_{thi0} \doteq \sqrt{T_0/m_i}$ is the reference ion thermal velocity.

The dimensionless viscosity, viscosity ratio, particle, and source and current, as well as the dimensionless primary small parameter, are given by

$$\tilde{\eta} \doteq \frac{\tilde{n}}{\sqrt{\tilde{T}_i}\tilde{B}^2}, \tag{17}$$

$$Q \doteq \frac{10\sqrt{2}\nu_{ie0}}{3\nu_{ii0}}, \tag{18}$$

$$\mathcal{P} \doteq \frac{1}{n_0 \rho_{i0}^2 \nu_{ie0}}\Gamma(R), \tag{19}$$

$$\mathcal{I} \doteq \frac{10\sqrt{2}R}{3Z_i e n_0 \rho_{i0}^3 \nu_{ii0}}C(R), \tag{20}$$

$$\delta = \frac{\rho_{i0}}{R}\frac{\tilde{E}}{\tilde{r}\tilde{B}^2}. \tag{21}$$

Quantities with the subscript 0 are constant reference quantities. The reference ion Larmor radius is defined as $\rho_{i0} \doteq v_{thi0}/\Omega_{i0}$, and the dimensionless ρ_{i0} is defined as $\rho_* \doteq \rho_{i0}/R$.

The solution to Eq. (15) is given as

$$\tilde{\omega}_{rot}(\tilde{r}) = e^{Q\mathcal{P}\int_1^{\tilde{r}}(\tilde{\Gamma}/\tilde{x}\tilde{\eta})d\tilde{x}}\left[\tilde{\omega}_{rot}|_{\tilde{r}=1} + \mathcal{I}\int_1^{\tilde{r}}\frac{e^{-Q\mathcal{P}\int_1^{\tilde{r}'}(\tilde{\Gamma}/\tilde{x}\tilde{\eta})d\tilde{x}}}{\tilde{r}'^3 \tilde{\eta}(\tilde{r}')}\right.$$
$$\left. \times \int_0^{\tilde{r}'}\tilde{y}\tilde{C}(\tilde{y})\tilde{B}(\tilde{y})d\tilde{y}d\tilde{r}'\right]. \tag{22}$$

One might notice that in order to keep $\mathcal{P}, \mathcal{I} \sim \mathcal{O}(1)$, the source terms must scale as $\tilde{s}_i \sim \rho_*^2$, $\sum_s Z_s \tilde{s}_s \sim \rho_*^3$.

Using Ampère's law, we can derive the ODE for the magnetic field strength to the same order of accuracy,

$$\tilde{B}' = \frac{\tilde{n}_i \tilde{r} \tilde{\omega}_{rot}^2 - (\tilde{p}'_i + \tilde{p}'_e)}{\tilde{v}_A^2 \tilde{B}}. \tag{23}$$

Here, the normalized Alfvén speed is defined as

$$\tilde{v}_A^2 \doteq \frac{B_0^2}{n_0 T_0 \mu_0} = \frac{2}{\beta}. \tag{24}$$

Equation (24) also shows the relation between $\tilde{v}_A^2$ and the plasma β.

Equation (23) can be integrated to yield

$$\tilde{B}(\tilde{r}) = \sqrt{\tilde{B}^2|_{\tilde{r}=0} + \frac{2}{\tilde{v}_A^2}\int_0^{\tilde{r}}\left(\tilde{n}_i\tilde{r}\tilde{\omega}_{rot}^2 - (\tilde{p}'_i + \tilde{p}'_e)\right)d\tilde{r}}, \tag{25}$$

where the constant of integration might be selected to satisfy $\int_0^1 \tilde{B}\tilde{r}d\tilde{r} = 1/2$, corresponding to a radial rearrangement of a magnetic field with initial uniform strength $\tilde{B} = 1$.

The boundary condition for (19) might be also selected for a set particle number $\tilde{N} = \int_0^1 \tilde{n}_i\tilde{r}d\tilde{r} = 1/2$, also corresponding to a radial rearrangement of a uniform particle density $\tilde{n}_i = 1$.

Kolmes et al.[30] plot (Fig. 3) the steady state normalized density, angular velocity, and viscosity distributions for four temperature profiles, for the case of uniform ion an electron particle sources ($\tilde{\Gamma} = \tilde{r}^2, \tilde{C} = \tilde{r}^2$), with $\mathcal{P} = 1$, $\mathcal{I} = -1$ and $Q = 0.1556$—corresponding to a proton fluid. That figure contains an error which Fig. 1 corrects.

IV. SIMULATION IN MITNS

As mentioned above, MITNS[46] is a numerical tool, capable of evolving the first three fluid moments for an arbitrary number of ion species, as well as Faraday's law.

A. Code details

It should be noted that the equation set solved by MITNS is somewhat different than the full model described in Sec. II; MITNS takes electrons into account only algebraically, as discussed in Appendix B, and so the electron inertial terms in the momentum equation do not appear. Electron viscosity is dropped as it is smaller than the ion viscosity by a factor $Z^3 m_e/m_i$ for the η_0 term,[47,48] by a factor of $Z^2 m_e/m_i$ for the η_3 term, and by a factor of $Z^4(m_e/m_i)^{3/2}$ for the η_1 term.[28] We concern ourselves with ionization numbers $Z < 5$. At larger values of Z, ionization/recombination effects might become relevant, and these are out of the scope of this work.

MITNS implements Eqs. (1)–(8) for the ions and the magnetic field, taking $\eta_0 \equiv 0$. The η_0 term ends up being ρ_*^2 smaller than the pressure gradient term in the radial momentum equation.

MITNS evaluates $\tilde{n}_s$, $\tilde{v}_{s\theta}$, $\tilde{p}_s$, and $\tilde{B}_z$ and their time derivatives at cell centers and as such avoids the coordinate singularity at $r = 0$, in the divergence terms $\text{div }\mathbf{V} = \frac{1}{r}\frac{\partial}{\partial r}rV_r$, and $(\text{div }\mathbf{T})\cdot\hat{\theta} = \frac{1}{r}[\frac{\partial}{\partial r}rT_{r\theta} + T_{\theta r}]$, for a vector quantity $\mathbf{V}$ and a tensor quantity $\mathbf{T}$. For v_r, since $v_r(0, t) = 0$ due to axisymmetry, there is no need to evaluate $\frac{\partial}{\partial t}v_r(0, t)$. For the viscous stress tensor, writing

$$r^3 \frac{\partial}{\partial r}\frac{v_\theta}{r} = r^2 v'_\theta - rv_\theta, \tag{26}$$

eliminates the need to evaluate v_θ/r at $r = 0$ in order to compute the viscous stress on the cell adjacent to $r = 0$.

A monotonized-central Van-Leer[49] flux limiter is employed for the particle and momentum fluxes, as well as the magnetic field flux, in an upwind scheme in order to avoid spurious oscillations.
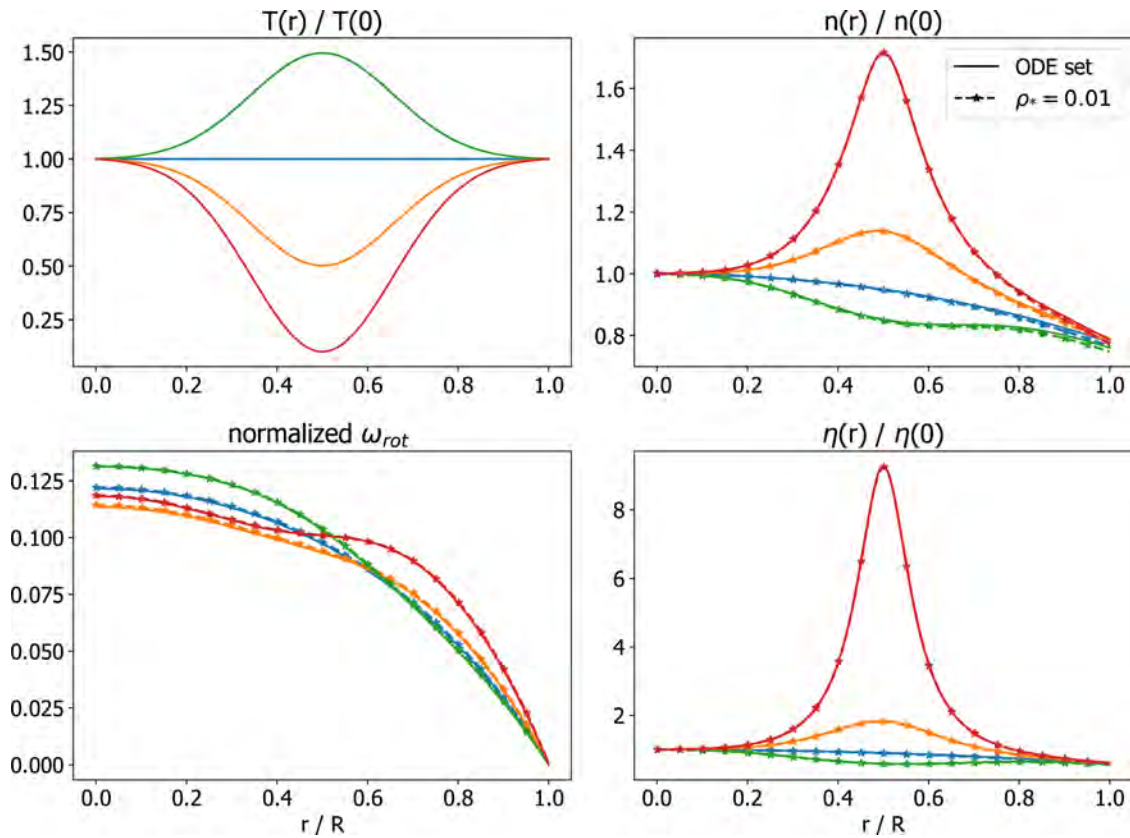
FIG. 1. Several solutions of the rotation profile, density, and viscosity coefficient corresponding to some steady state temperature profiles, $\mathcal{P} = 1$, $\mathcal{I} = -1$, $\mathcal{Q} = 0.1556$. Comparison between MITNS results, for reference normalized ion Larmor radius $\rho_* = 0.01$. Markers ($\star$) are placed every 30 grid points for MITNS solution, $\rho_* = 0.01$ for visibility. Notice the agreement between the normalized (first order) angular velocity from the ODE set (full line) and the angular velocity profile from MITNS (dashed line with markers) at the bottom-left plot.

B. Simulation details

In order to verify MITNS' solution in cylindrical coordinates, we attempt to simulate the same scenario as was presented in Kolmes *et al.*[30] That paper dealt with the momentum equation only for an electron and proton fluids, in steady state. As long as the temperature remains close to the reference temperature, rather than gain or lose factors of ρ_*, the asymptotic expansion in Kolmes *et al.*[30] holds, and the momentum equation describes adequately the momentum and charge transport, for given a temperature profile. To do so, the pressure equation was disabled in MITNS, and a temperature profile was prescribed, $T_p = T_e = T(r,t)$. Here, we consider a singly ionized electron-proton plasma, and use the subscript p for the proton fluid. The momentum equation and the continuity equation for a proton fluid were integrated in time.

The initial conditions for the simulation were $\tilde{n}_p \equiv 1$, $\tilde{v}_{pr} \equiv 0$, $\tilde{v}_{p\theta} \equiv 0$, and $\tilde{B}_z \equiv 1$.

Volumetric sources and conditions: the proton and electron temperatures profiles were prescribed as $\tilde{T}_p(\tilde{t}, \tilde{r}) = \tilde{T}_e(\tilde{t}, \tilde{r}) = 1 + T_* \tanh^4(t/t_{rise}) e^{-20(\tilde{r}-0.5)^2}$, with the parameter $T_* \in \{0, 0.5, -0.5, -0.9\}$ for the four cases presented in Fig. 1.

The volumetric proton source term uniform across the computational box and had the same time dependence $\tilde{s}_p(t) = \tilde{s}_* \tanh^4(t/t_{rise})$ for a value of $\tilde{s}_*$ such that $\mathcal{P} = 1$ according to Eq. (19).

The electron source term affects the radial electron velocity, as discussed in Appendix B, in Eq. (B4). It was set such that $\tilde{j}_r = \tilde{j}_{r*} \tilde{r} \tanh^4(5t/t_{rise})$ for a value of $\tilde{j}_{r*}$ such that $\mathcal{C} = -1$ according to Eq. (20).

The proton and electron injection velocities, $\tilde{v}^{src}$, as appearing in the momentum source in Eq. (2), were zero.

The boundary conditions were: the proton velocity was determined through the flux, $\tilde{\Gamma}_p(\tilde{t}, 1) = \int_0^1 \tilde{r}' \tilde{s}_p(\tilde{t}, \tilde{r}') d\tilde{r}'$, that is, the proton and electron, (due to quasi-neutrality) total number was kept constant—the adjective flux out of the computational box was matched to the volumetric particle source. The radial velocity at $\tilde{r} = 0$ is $\tilde{v}_{sr}(\tilde{t}, 0) \equiv 0$ due to axisymmetry.

A zero advective magnetic field flux boundary condition was set on the outer radius of the domain, such that the total magnetic flux in the domain remains constant.

These boundary conditions and source terms were evolved until a steady state was achieved.

The dimensionless parameters realized in this simulation are summarized in Table I.

The results of these simulation are of a driven steady state, with (constant) proton and electron source terms that result in a (stationary) radial current. This current produces a constant $\mathbf{j} \times \mathbf{B}$ torque, which is balanced by ion viscosity.

TABLE I. Dimensionless parameters. Knudsen number, $Kn = v_{th0}/\nu L$, depends on the length L of the cylinder (along field lines), which is not used and can be arbitrarily long.

Parameter	Symbol	Value
Proton normalized Larmor radius	ρ_*	0.01
Proton–proton Hall parameter	Ω_p/ν_{pp}	14
Proton–electron Hall parameter	Ω_p/ν_{pe}	433
Plasma β	B	0.002
Reynolds number	Re	35
Magnetic Reynolds number	Rm	220

The pressure equation is not solved in this simulation, even though it is included in MITNS, as the purpose of this work is to test the numerical solution against an analytic one, which present a solution to the momentum equation. The steady state velocity profiles discussed in this paper would generate viscous and frictional heating. We assume that the temperature can be controlled via some external mechanism, such as tailoring the injected particles temperature, or some form of radiative cooling. The effects involving the heating channels and the pressure evolution will be pursued in a future work.

C. Magnetic field evolution

The magnetic field evolution in MITNS is determined by Faraday's law,

$$\frac{\partial B_z}{\partial t} = -\frac{1}{r}\frac{\partial}{\partial r}rE_\theta = -\frac{1}{r}\frac{\partial}{\partial r}r\left[v_{er}B_z + \sum_s\left(\frac{m_e\nu_{es}}{e}(v_{s\theta} - v_{e\theta}) + \frac{f_{es}}{en_e}\right)\right],$$
(27)

where the electric field is determined by the electron momentum equation, as seen in the second line of Eq. (27).

In steady state, the $v_{er}B_z$ term and the friction and Nernst force terms balance each other. In this simulation, particles are injected in to the simulation domain, which generates radial particle fluxes. These radial particle fluxes generate torques, which then produce angular velocity in the fluids. This means that before steady state is established, the advection term, which depends on the radial electron flux, is larger than the azimuthal term in (27), and magnetic field is pushed out initially.

Without imposing zero magnetic field flux out of the outer radius, this would lead to some magnetic field leaving the computation domain, and thus being lost. Electron-ion friction provides magnetic field diffusion and prevents it from piling up at edge of the domain in steady state.

The steady state radial current produces a steady state (and larger) azimuthal current. This current would keep B_z nonuniform.

It is possible to have an annular domain and inject particles only through the inner boundary instead of volumetrically. In that case, an appropriate set of coils around the inner electrode could ensure the edge source of electrons carry magnetic field into the domain, which would replenish the initial magnetic field loss. This setup would produce a different torque on the plasma $\tau = \mathbf{r} \times (\mathbf{j} \times \mathbf{B}) \propto B_z$ rather than $\propto r^2 B_z$, which would be balanced by a different viscous stress profile, and hence a different angular velocity profile.

D. Comparison of analytic transport theory with MITNS

A comparison between the solution to Eqs. (15) and (16), produced as an asymptotic expansion in small parameters δ, ϵ, and the steady-state results of a simulation in MITNS is presented in Fig. 1. The small parameter ρ_* is set by specifying the domain size in MITNS, and δ Eq. (10), depends on it, together with the electric and magnetic fields produced as a result of the applied sources and boundary conditions. A comparison between the magnetic field given by Eq. (25), and the one solved for in MITNS is shown in Fig. 2, for the same simulations presented in Fig. 1.

There is a good agreement between the ODE set solution and the steady-state MITNS result for $\rho_* = 0.01$, as evidenced by the closeness of the dashed and full lines in Figs. 1 and 2. The small parameter, $|\delta(r)|$, in this case was <0.002.

V. ANGULAR-MOMENTUM TRANSPORT VIEW OF RADIAL CURRENTS

Interestingly, comparing the expression $-E/rB$ evaluated by MITNS, as shown in Fig. 3, to the angular velocity profile in Fig. 1 shows there are some differences between them, when solving the system of equations for a small but finite ρ_*. The $\mathbf{E} \times \mathbf{B}$ azimuthal drift discussed in Kolmes et al.[30] is recovered in the limit of $\rho_* \to 0$.

For the $\rho_* = 0.01$ case, the most visible features in Fig. 3 are the nonzero derivative at $r = 0$, and the nonmonotonicity of the green curve, even though the angular velocity profile is monotonic in Fig. 1. This means that the solution to Eq. (15) contains information about the diamagnetic drift as well as $-E/rB$.

In this section, we aim to expand upon the ordering of the equations of motion for N-fluids, derive the angular velocity and density profiles in terms of the cross field particle fluxes, and show the solution presented in Sec. III is a particular solution obtained for a specific ordering of the particle flux magnitude. The small parameters in the expansion presented in this section are formally constants, rather than a function of the solution, which is easier to handle. Additionally, we explicitly keep the inner boundary terms such as in Eqs. (29), (36), and (37), which are set to zero in Kolmes et al.[30] Eq. (48), for example.
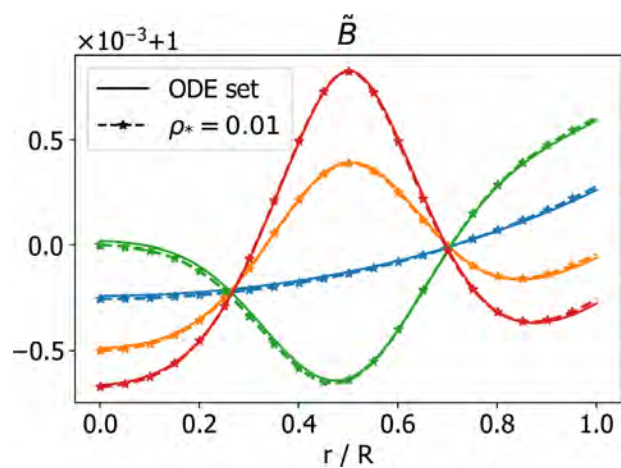

FIG. 2. Comparison between Eq. (25) and MITNS solution for the dimensionless magnetic field, for the same cases presented in Fig. 1, using $\tilde{v}_A^2 = 1000$.
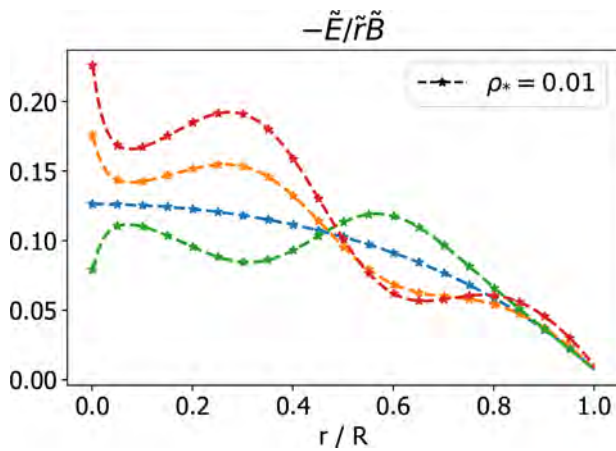
FIG. 3. MITNS calculated dimensionless $-E/rB$ for the same cases presented in Fig. 1. Large disagreements between the dimensionless first-order rotation frequency in Fig. 1 and the resultant electric field here.

These boundary terms would be useful in annular geometries used for homopolar generators or some mass filter applications.

Writing the equations of motion in term of angular momentum, rather than linear momentum, casts the viscous torque term in a diffusion form. This form enables the angular momentum equation to be written in a finite-volume form, which is computationally conservative scheme.

The continuity equation and the radial particle flux,

$$\frac{\partial n_s}{\partial t} + \frac{1}{r}\frac{\partial}{\partial r}\Gamma_s = s_s, \tag{28}$$

$$\Gamma_s = rn_s v_{sr} = \Gamma_s(r_i) + \int_{r_i}^{r}\left(s_s - \frac{\partial n_s}{\partial t}\right)r'dr', \tag{29}$$

are the driving mechanisms for the system dynamics, and they are a reasonable boundary condition to experimentally impose.

The angular momentum conservation equation,

$$\ell_s \doteq rm_s n_s v_{s\theta} = \mathbf{r}\times\mathbf{P}_s\cdot\hat{z}, \tag{30}$$

$$\frac{\partial \ell_s}{\partial t} + \frac{1}{r}\frac{\partial}{\partial r}\frac{\ell_s\Gamma_s}{n_s} + Z_s e\Gamma_s B_z$$
$$= \sum_{s'}(\nu_{s's}\ell_{s'} - \nu_{ss'}\ell_s) + \frac{1}{r}\frac{\partial}{\partial r}r^3\left[\eta_{s1}\omega_s' - \eta_{s3}\frac{\partial}{\partial r}\left(\frac{\Gamma_s}{r^2 n_s}\right)\right]$$
$$+ r\sum_{s'}f_{ss'\theta} + \ell_s^{src}, \tag{31}$$

is written here as an advection–diffusion equation for each species, with source terms corresponding to the Lorentz torque on the left-hand side, and the friction and Nernst torques on the right-hand side. The last term, ℓ_s^{src}, indicates other sources of angular momentum, such as the injection of particles with nonzero angular velocity. In that case, $\ell_s^{src} = r^2 m_s s_s \omega_s^{src}$. We shall take this term to be zero from now.

The radial component of the momentum equation, for $P_{sr} \doteq m_s n_s v_{sr}$,

$$\frac{\partial P_{sr}}{\partial t} + \frac{1}{r}\frac{\partial}{\partial r}rP_{sr}v_{sr} + p_s' = \frac{1}{r}\ell_s\omega_s + Z_s en_s(E_r + r\omega_s B_z)$$
$$+ \sum_{s'}(\nu_{s's}P_{s'r} - \nu_{ss'}P_{sr}) + \frac{\partial}{\partial r}\left[\frac{\eta_{s0}}{3r}\frac{\partial}{\partial r}(rv_{sr})\right]$$
$$+ \frac{1}{r^2}\frac{\partial}{\partial r}r^3\left[\eta_{s1}\frac{\partial}{\partial r}\left(\frac{v_{sr}}{r}\right) + \eta_{s3}\omega_s'\right] + P_{sr}^{src}, \tag{32}$$

can be written in a form such that the viscosity is a diffusion term. However, writing this equation in that form introduces source terms relating to the pressure, momentum, and the η_0 component of viscosity.

Using

$$M_s \doteq rm_s n_s v_{sr} = \mathbf{r}\cdot\mathbf{P}_s = m_s\Gamma_s, \tag{33}$$

the conservation equation for M_s is

$$\frac{\partial M_s}{\partial t} + \frac{1}{r}\frac{\partial}{\partial r}\left(\frac{M_s\Gamma_s}{n_s} + r^2 p_s\right)$$
$$= 2p_s + \frac{M_s\Gamma_s}{r^2 n_s} + \omega_s\ell_s + Z_s en_s r(E_r + r\omega_s B_z)$$
$$+ \sum_{s'}(\nu_{s's}M_{s'} - \nu_{ss'}M_s) + \frac{1}{r}\frac{\partial}{\partial r}r^3\left[\eta_{s1}\frac{\partial}{\partial r}\left(\frac{\Gamma_s}{r^2 n_s}\right) + \eta_{s3}\omega_s'\right]$$
$$+ \frac{1}{r}\frac{\partial}{\partial r}\left[\frac{r\eta_{s0}}{3}\frac{\partial}{\partial r}\left(\frac{\Gamma_s}{n_s}\right)\right] - \frac{2\eta_{s0}}{3r}\frac{\partial}{\partial r}\left(\frac{\Gamma_s}{n_s}\right) + M_s^{src}. \tag{34}$$

The integral form of the Eq. (31) is

$$\frac{\partial}{\partial t}\int_{r_i}^{r}\ell_s r'dr' + \frac{\ell_s\Gamma_s}{n_s}\bigg|_{r_i}^{r} + Z_s e\int_{r_i}^{r}\Gamma_s B_z r'dr'$$
$$= \sum_{s'}\int_{r_i}^{r}\left(\nu_{s's}\ell_{s'} - \nu_{ss'}\ell_s + f_{ss'\theta}r'\right)r'dr'$$
$$+ r^3\left[\eta_{s1}\omega_s' - \eta_{s3}\frac{\partial}{\partial r}\left(\frac{\Gamma_s}{r^2 n_s}\right)\right]_{r_i}^{r}, \tag{35}$$

where integrals of the form $\int_{r_i}^{r}\cdot r'dr'$ should be understood as volume average in the annular volume bounded by r_i and r.

Summing over all species in steady state, the friction forces cancel, and the electric field term drops off due to quasi-neutrality.

$$\sum_s m_s r^2\omega_s\Gamma_s\big|_{r_i}^{r} + \int_{r_i}^{r}CB_z r'dr'$$
$$= \sum_s r^3\left[\eta_{s1}\omega_s' - \eta_{s3}\frac{\partial}{\partial r}\left(\frac{\Gamma_s}{r^2 n_s}\right)\right]_{r_i}^{r}, \tag{36}$$

$$\sum_s\frac{1}{r}\frac{\partial}{\partial r}\left(\frac{m_s\Gamma_s^2}{n_s} + r^2 p_s\right)$$
$$= \sum_s\left[2p_s + \frac{m_s\Gamma_s^2}{r^2 n_s} + \omega_s\ell_s\right]$$
$$+ \sum_s Z_s en_s r^2\omega_s B_z + \sum_s\frac{1}{r}\frac{\partial}{\partial r}r^3\left[\eta_{s1}\frac{\partial}{\partial r}\left(\frac{\Gamma_s}{r^2 n_s}\right) + \eta_{s3}\omega_s'\right]$$
$$+ \sum_s\frac{1}{r}\frac{\partial}{\partial r}\left[\frac{r\eta_{s0}}{3}\frac{\partial}{\partial r}\left(\frac{\Gamma_s}{n_s}\right)\right] - \sum_s\frac{2\eta_{s0}}{3r}\frac{\partial}{\partial r}\left(\frac{\Gamma_s}{n_s}\right). \tag{37}$$

These equations do not depend on the electric field, and we will show their equivalence to Eqs. (15) and (16). The leading order ω, even though it must be of $\mathcal{O}\left(\frac{E}{rB}\right)$, by the choice of the Braginskii transport coefficients may contain information from other particle drifts.

A. Nondimensionalization

Nondimensionalizing the equations of motion would factor out small parameters that would be used in an asymptotic expansion.

Denoting $X = X_0\tilde{X}$, with X_0 being a reference quantity,

$$m_0 \doteq m_p, \tag{38}$$

$$v_0 \doteq \sqrt{T_0/m_p}, \tag{39}$$

$$r_0 \doteq R, \tag{40}$$

$$\Gamma_0 \doteq Rn_0 v_0, \tag{41}$$

$$C_0 \doteq eRn_0 v_0, \tag{42}$$

$$\eta_{30} \doteq \frac{n_0 T_0}{\Omega_{p0}}, \tag{43}$$

$$\eta_{10} \doteq \frac{n_0 T_0 \nu_0}{\Omega_{p0}^2}, \tag{44}$$

$$\eta_{00} \doteq \frac{n_0 T_0}{\nu_0}, \tag{45}$$

$$R_{ss'0} \doteq m_0 n_0 \nu_0 v_0, \tag{46}$$

$$f_{ss'0} \doteq \frac{n_0 \nu_0 T_0}{\Omega_{p0} R} = m_0 n_0 \nu_0 v_0 \rho_*, \tag{47}$$

with R being the outer domain radius.

The dimensionless equations feature the two small parameters $\rho_* \doteq v_0/\Omega_{p0}R$ and $\epsilon \doteq \nu_0/\Omega_{p0}$. They are ordered such that $1 \gg \epsilon \gg \rho_*$.

The steady-state dimensionless angular momentum for a single fluid species is

$$\tilde{m}_s \tilde{r}^2 \tilde{\Gamma}_s \tilde{\omega}_s \big|_{\tilde{r}_i}^{\tilde{r}} + \frac{1}{\rho_*} \int_{\tilde{r}_i}^{\tilde{r}} Z_s \tilde{r}' \tilde{\Gamma}_s \tilde{B}_z d\tilde{r}'$$
$$= \rho_* \tilde{r}^3 \left[\epsilon \tilde{\eta}_{s1} \tilde{\omega}_s' - \tilde{\eta}_{s3} \frac{\partial}{\partial \tilde{r}} \left(\frac{\tilde{\Gamma}_s}{\tilde{r}^2 \tilde{n}_s} \right) \right] \Big|_{\tilde{r}_i}^{\tilde{r}}$$
$$+ \epsilon \int_{\tilde{r}_i}^{\tilde{r}} \sum_{s'} \left(\frac{1}{\rho_*} \tilde{R}_{ss'\theta} + \tilde{f}_{ss'\theta} \right) \tilde{r}'^2 d\tilde{r}'. \tag{48}$$

The equation for the entire plasma is

$$\sum_s \tilde{m}_s \tilde{r}^2 \tilde{\Gamma}_s \tilde{\omega}_s \big|_{\tilde{r}_i}^{\tilde{r}} = \rho_* \epsilon \tilde{r}^3 \sum_s \tilde{\eta}_{s1} \tilde{\omega}_s' \big|_{\tilde{r}_i}^{\tilde{r}}$$
$$- \rho_* \tilde{r}^3 \sum_s \tilde{\eta}_{s3} \frac{\partial}{\partial \tilde{r}} \left(\frac{\tilde{\Gamma}_s}{\tilde{r}^2 \tilde{n}_s} \right) \Big|_{\tilde{r}_i}^{\tilde{r}} - \frac{1}{\rho_*} \int_{\tilde{r}_i}^{\tilde{r}} \tilde{r}' \tilde{C} \tilde{B}_z d\tilde{r}'. \tag{49}$$

We shall order the angular velocity and source terms in the two small parameters using $\tilde{X} = \sum_{\alpha,\beta} \rho_*^\alpha \epsilon^\beta \tilde{X}^{(\alpha,\beta)}$ and restrict $\tilde{\omega}_s$ such that its leading term is $\tilde{\omega}_s^{(0,0)}$.

Equation (48), when expanded to $\mathcal{O}(\rho_*^k)$, $k = -1, 0$, yields

$$\int_{\tilde{r}_i}^{\tilde{r}} Z_s \tilde{r}' \tilde{\Gamma}_s^{(k+1,0)} \tilde{B}_z d\tilde{r}' = 0, \tag{50}$$

$$\tilde{\Gamma}_s^{(0,0)} = \tilde{\Gamma}_s^{(1,0)} = 0. \tag{51}$$

To $\mathcal{O}(\rho_*^{-1}\epsilon)$,

$$Z_s \tilde{\Gamma}_s^{(0,1)} \tilde{B}_z = \sum_{s'} \left(\tilde{m}_s \tilde{n}_s \tilde{\nu}_{ss'} \tilde{r} (\tilde{\omega}_{s'}^{(0,0)} - \tilde{\omega}_s^{(0,0)}) + \tilde{f}_{ss'\theta}^{(-1,0)} \right) \tilde{r}. \tag{52}$$

Here, $\tilde{f}_{ss'\theta}^{(-1,0)}$ is understood as the dimensionless (4) with dimensionless temperature gradients of $\mathcal{O}(\rho_*^{-1})$.

To $\mathcal{O}(\epsilon)$,

$$\int_{\tilde{r}_i}^{\tilde{r}} \sum_{s'} \left(\tilde{r} \tilde{m}_s \tilde{n}_s \tilde{\nu}_{ss'} (\tilde{\omega}_{s'}^{(1,0)} - \tilde{\omega}_s^{(1,0)}) + \tilde{f}_{ss'\theta}^{(0,0)} \right) \tilde{r}'^2 d\tilde{r}'$$
$$= \tilde{r}^2 \tilde{m}_s \left[\tilde{\Gamma}_s^{(0,1)} \tilde{\omega}_s^{(0,0)} \right]_{\tilde{r}_i}^{\tilde{r}} + \int_{r_i}^r Z_s \tilde{r}' \tilde{\Gamma}_s^{(1,1)} \tilde{B}_z d\tilde{r}'. \tag{53}$$

This equation is the equivalent to Eq. (16), assuming the leading order $\tilde{\Gamma}_s$ is $\tilde{\Gamma}_s^{(1,1)}$.

Equation (49), when expanded to $\mathcal{O}(\rho_*^k)$, $k = -1, 0, 1$, yield

$$\int_{\tilde{r}_i}^{\tilde{r}} \tilde{r}' \tilde{C}^{(k+1,0)} \tilde{B}_z d\tilde{r}' = 0, \tag{54}$$

$$\tilde{C}^{(0,0)} = \tilde{C}^{(1,0)} = \tilde{C}^{(2,0)} = 0, \tag{55}$$

and when expanded to $\mathcal{O}(\rho_* \epsilon)$,

$$\tilde{r}^2 \sum_s \tilde{m}_s \left[\tilde{\Gamma}_s^{(1,1)} \tilde{\omega}_s^{(0,0)} + \tilde{\Gamma}_s^{(0,1)} \tilde{\omega}_s^{(1,0)} \right]_{\tilde{r}_i}^{\tilde{r}}$$
$$= \tilde{r}^3 \sum_s \tilde{\eta}_{s1} \tilde{\omega}_s^{(0,0)'} \big|_{\tilde{r}_i}^{\tilde{r}} - \tilde{r}^3 \sum_s \tilde{\eta}_{s3} \frac{\partial}{\partial \tilde{r}} \left(\frac{\tilde{\Gamma}_s^{(0,1)}}{\tilde{r}^2 \tilde{n}_s} \right) \Big|_{\tilde{r}_i}^{\tilde{r}}$$
$$- \int_{\tilde{r}_i}^{\tilde{r}} \tilde{r}' \tilde{C}^{(2,1)} \tilde{B}_z d\tilde{r}'. \tag{56}$$

Equation (56) is the differential equation for $\tilde{\omega}_s^{(0,0)}$, assuming $\tilde{C} = \rho_*^2 \epsilon \tilde{C}^{(2,1)}$, and $\tilde{\Gamma}_s = \rho_* \epsilon \tilde{\Gamma}_s^{(1,1)}$, are known functions. If $\tilde{r}_i = 0$, it reduces to (15).

To $\mathcal{O}(\rho_*^2 \epsilon)$,

$$\tilde{r}^2 \sum_s \tilde{m}_s \left[\tilde{\Gamma}_s^{(2,1)} \tilde{\omega}_s^{(0,0)} + \tilde{\Gamma}_s^{(0,1)} \tilde{\omega}_s^{(2,0)} + \tilde{\Gamma}_s^{(1,1)} \tilde{\omega}_s^{(1,0)} \right]_{\tilde{r}_i}^{\tilde{r}}$$
$$+ \tilde{r}^3 \sum_s \tilde{\eta}_{s3} \frac{\partial}{\partial \tilde{r}} \left(\frac{\tilde{\Gamma}_s^{(1,1)}}{\tilde{r}^2 \tilde{n}_s} \right) \Big|_{\tilde{r}_i}^{\tilde{r}} + \int_{\tilde{r}_i}^{\tilde{r}} \tilde{r}' \tilde{C}^{(3,1)} \tilde{B}_z d\tilde{r}'$$
$$= \tilde{r}^3 \sum_s \tilde{\eta}_{s1} \tilde{\omega}_s^{(1,0)'} \big|_{\tilde{r}_i}^{\tilde{r}} - \tilde{r}^2 \sum_s \tilde{m}_s \left[\tilde{\Gamma}_s^{(2,0)} \tilde{\omega}_s^{(0,1)} \right]_{\tilde{r}_i}^{\tilde{r}}. \tag{57}$$

This becomes the differential equation for $\tilde{\omega}_s^{(1,0)}$, assuming $\tilde{C} = \rho_*^2 \epsilon \tilde{C}^{(2,1)}$, and $\tilde{\Gamma}_s = \rho_* \epsilon \tilde{\Gamma}_s^{(1,1)}$, are known functions,

$$\sum_s \tilde{m}_s \left[\tilde{\Gamma}_s^{(1,1)} \tilde{\omega}_s^{(1,0)} \right]_{\tilde{r}_i}^{\tilde{r}} + \tilde{r} \sum_s \tilde{\eta}_{s3} \frac{\partial}{\partial \tilde{r}} \left(\frac{\tilde{\Gamma}_s^{(1,1)}}{\tilde{r}^2 \tilde{n}_s} \right) \Big|_{\tilde{r}_i}^{\tilde{r}}$$
$$= \tilde{r} \sum_s \tilde{\eta}_{s1} \tilde{\omega}_s^{(1,0)'} \big|_{\tilde{r}_i}^{\tilde{r}}. \tag{58}$$

The dimensionless steady-state mass flux equation for a single fluid species is

$$\frac{1}{\tilde{r}}\frac{\partial}{\partial \tilde{r}}\left(\frac{\tilde{m}_s \tilde{\Gamma}_s^2}{\tilde{n}_s} + \tilde{r}^2 \tilde{p}_s\right)$$

$$= 2\tilde{p}_s + \frac{\tilde{m}_s \tilde{\Gamma}_s^2}{\tilde{r}^2 \tilde{n}_s} + \tilde{m}_s \tilde{n}_s \tilde{r}^2 \tilde{\omega}_s^2 + \frac{1}{\rho_*}Z_s \tilde{n}_s \tilde{r}\left(\tilde{E}_r + \tilde{r}\tilde{\omega}_s \tilde{B}_z\right)$$

$$+ \frac{\epsilon}{\rho_*}\sum_{s'}\left(\tilde{m}_{s'}\tilde{\nu}_{s's}\tilde{\Gamma}_{s'} - \tilde{m}_s \tilde{\nu}_{ss'}\tilde{\Gamma}_s\right)$$

$$+ \frac{\rho_*}{\tilde{r}}\frac{\partial}{\partial \tilde{r}}\tilde{r}^3\left[\epsilon \tilde{\eta}_{s1}\frac{\partial}{\partial \tilde{r}}\left(\frac{\tilde{\Gamma}_s}{\tilde{r}^2 \tilde{n}_s}\right) + \tilde{\eta}_{s3}\tilde{\omega}_s'\right]$$

$$+ \frac{\rho_*}{\epsilon}\frac{1}{\tilde{r}}\frac{\partial}{\partial \tilde{r}}\left[\frac{\tilde{r}\tilde{\eta}_{s0}}{3}\frac{\partial}{\partial \tilde{r}}\left(\frac{\tilde{\Gamma}_s}{\tilde{n}_s}\right)\right] - \frac{\rho_*}{\epsilon}\frac{2\tilde{\eta}_{s0}}{3\tilde{r}}\frac{\partial}{\partial \tilde{r}}\left(\frac{\tilde{\Gamma}_s}{\tilde{n}_s}\right). \qquad (59)$$

To leading order, $\mathcal{O}(\rho_*^{-1})$,

$$\tilde{p}_s^{(-1,0)'} = Z_s \tilde{n}_s\left(\tilde{E}_r^{(0,0)} + \tilde{r}\tilde{\omega}_s^{(0,0)}\tilde{B}_z\right), \qquad (60)$$

where $\tilde{p}_s^{(-1,0)'}$ is understood as resulting from temperature gradients that are of $\mathcal{O}(\rho_*^{-1})$.

Equation (60) is deceptive, as it seems to imply the leading order rotation is an $\mathbf{E} \times \mathbf{B}$ drift. However, one arrives at this equation after solving for $\tilde{\omega}_s^{(0,0)}$. This equation actually defines the electric field profile. This assertion is reflected in Fig. 4, which compares $\tilde{\omega}_{rot}$, the electric field (appears in Fig. 3) and the pressure gradient terms (appears in Fig. 5 and must be multiplied by ρ_* to convert from $\tilde{p}'/\tilde{r}\tilde{n}\tilde{B}$ to $\tilde{p}^{(-1,0)'}/\tilde{r}\tilde{n}\tilde{B}$). The sum of the nonmonotonic pressure gradient and electric field terms cancel each other such that the remainder is the monotonic angular velocity everywhere except right next to the origin.

To $\mathcal{O}(1)$, subtracting Eq. (59) for $s = s'$ from itself with $s = s$,

$$\tilde{\omega}_{s'}^{(1,0)} - \tilde{\omega}_s^{(1,0)} = \frac{\tilde{p}_{s'}^{(0,0)}}{Z_{s'}\tilde{n}_{s'}\tilde{r}\tilde{B}_z} - \frac{\tilde{m}_{s'}\tilde{\omega}_{s'}^{(0,0)2}}{Z_{s'}\tilde{B}_z} - \frac{\tilde{p}_s^{(0,0)}}{Z_s\tilde{n}_s\tilde{r}\tilde{B}_z} + \frac{\tilde{m}_s\tilde{\omega}_s^{(0,0)2}}{Z_s\tilde{B}_z}, \qquad (61)$$

allows us to achieve a nonambiguous expression, to be substituted in Eq. (53).

The dimensionless form of Eq. (37) is

$$\sum_s \frac{1}{\tilde{r}}\frac{\partial}{\partial \tilde{r}}\left(\frac{\tilde{m}_s \tilde{\Gamma}_s^2}{\tilde{n}_s} + \tilde{r}^2 \tilde{p}_s\right)$$

$$= \sum_s\left[2\tilde{p}_s + \frac{\tilde{m}_s \tilde{\Gamma}_s^2}{\tilde{r}^2 \tilde{n}_s} + \tilde{m}_s \tilde{n}_s \tilde{\omega}_s^2 \tilde{r}'^2\right] + \frac{1}{\rho_*}\sum_s Z_s \tilde{n}_s \tilde{r}^2 \tilde{\omega}_s \tilde{B}_z$$

$$+ \rho_* \sum_s \frac{1}{\tilde{r}}\frac{\partial}{\partial \tilde{r}}\tilde{r}^3\left[\epsilon \tilde{\eta}_{s1}\frac{\partial}{\partial \tilde{r}}\left(\frac{\tilde{\Gamma}_s}{\tilde{r}^2 \tilde{n}_s}\right) + \tilde{\eta}_{s3}\tilde{\omega}_s'\right]$$

$$+ \sum_s \frac{\rho_*}{\epsilon}\frac{1}{\tilde{r}}\frac{\partial}{\partial \tilde{r}}\left[\frac{\tilde{r}\tilde{\eta}_{s0}}{3}\frac{\partial}{\partial \tilde{r}}\left(\frac{\tilde{\Gamma}_s}{\tilde{n}_s}\right)\right] - \sum_s \frac{\rho_*}{\epsilon}\frac{2\tilde{\eta}_{s0}}{3\tilde{r}}\frac{\partial}{\partial \tilde{r}}\left(\frac{\tilde{\Gamma}_s}{\tilde{n}_s}\right). \qquad (62)$$

To leading order, using Ampère's law, this is an equation for the magnetic field,

$$\sum_s \tilde{p}_s' + \tilde{r}\tilde{\omega}_s^{(0,0)2}\sum_s \tilde{m}_s \tilde{n}_s = \mu_0^{-1}\frac{\partial \tilde{B}_z^{(1,0)}}{\partial \tilde{r}}\tilde{B}_z. \qquad (63)$$

In this section, we derived the leading and first-order correction equations for the angular velocity profile, and the leading order equations for the density and magnetic field. We have shown how different particle flux magnitudes affect the solution, and suggested an interpretation of the relation between the leading order rotation and the electric field.

VI. CONCLUSION

The code MITNS, Multiple-Ion Transport Numerical Solver, was expanded to include a cylindrical coordinate mode and used to validate the first-order solution to the rotation frequency and density distribution in a source-driven, axially magnetized, rotating two-fluid plasma cylinder presented in Kolmes *et al.*[30]

First, simulation results pointed to the error in the plotting script for Fig. 3 in Ref. 30, and we were able to correct it in Fig. 1.

Second, we have shown the approach to steady-state should be performed carefully, with appropriate magnetic boundary conditions,
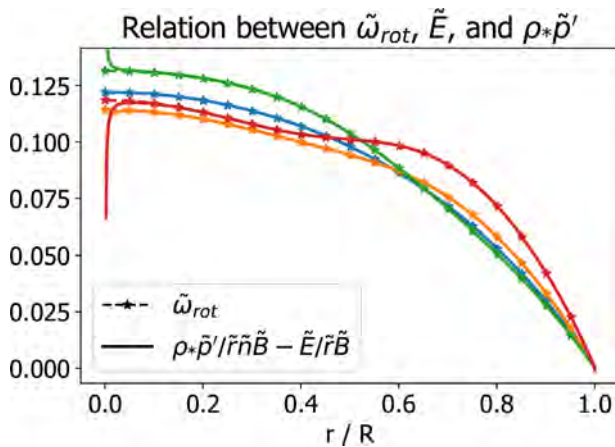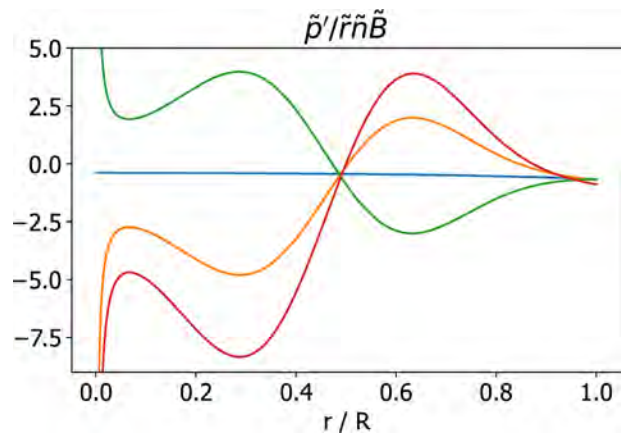

FIG. 4. Comparison between $\tilde{\omega}_{rot}$, electric field and the pressure gradient terms from Eq. (60), as calculated by MITNS for the same cases presented in Fig. 1.

FIG. 5. ODE set calculated dimensionless diamagnetic angular velocity.

or else particle fluxes out of the simulation domain will deplete the magnetic field.

Third, after requiring a constant magnetic flux in the cylinder, the results of the MITNS code and the ODE set solution were shown to be congruent in the limit of small Larmor radius over domain size. This lends credibility to the MITNS code and its cylindrical coordinates mode.

Finally, we derived the rotation frequency, density, and magnetic field equations and suggested an interpretation to the relation between the electric field and rotation profile.

ACKNOWLEDGMENTS

AUTHOR DECLARATIONS
Conflict of Interest

The authors have no conflicts to disclose.

DATA AVAILABILITY

The data that support the findings of this study are available from the corresponding author upon reasonable request.

APPENDIX A: USING THE PARTICLE SOURCE-TERM AS A PROXY FOR THE AXIAL DIMENSION

In a steady state, azimuthally symmetric cylinder and in the absence of particle source terms, the continuity equation can be written as

$$\nabla \cdot (n_s \mathbf{v}_s) = \frac{1}{r}\frac{\partial}{\partial r}(r n_s v_{sr}) + \frac{\partial}{\partial z}(n_s v_{sz}) = s_s^{\text{source}}, \qquad (A1)$$

in the presence of fusion or ionization/recombination processes. s_s^{source} should be understood as a charge preserving in the sense $\sum_s Z_s s_s^{\text{source}} = 0$. This would lead to $C(r) \equiv 0$ in a cylinder or $C(r) \propto 1/r$ in an annulus, as defined in Eq. (13).

We are interested in the result of radial variation, so we can treat the $\frac{\partial}{\partial z}$ part of the divergence as an additional source term,

$$\frac{1}{r}\frac{\partial}{\partial r}(r n_s v_{sr}) = s_s = s_s^{\text{source}} - \frac{\partial}{\partial z}(n_s v_{sz}). \qquad (A2)$$

Identifying part of the source term with out-of-plane flow allows for charge/current source, where the electric charge weighted sum of electron and ion sources and sinks does not sum to zero.

Similarly, for the momentum equation, we have a degree of freedom in $\mathbf{v}_s^{src}$. Noticing the $\frac{\partial}{\partial z}$ component of $n_s(\mathbf{v}_s \cdot \nabla)\mathbf{v}_s$ is $n_s v_z \frac{\partial \mathbf{v}_s}{\partial z}$, we can choose $\mathbf{v}_s^{src}$ such that

$$\mathbf{v}_s^{src} = \mathbf{v} + \frac{n_s v_{sz}}{\frac{\partial}{\partial z}(n_s v_{sz}) - s_s^{\text{source}}}\frac{\partial \mathbf{v}}{\partial z} = \mathbf{v} - \frac{n_s v_{sz}}{s_s}\frac{\partial \mathbf{v}}{\partial z}. \qquad (A3)$$

Interpretation of the particle and velocity source terms as Eqs. (A2) and (A3) allows us to solve for 2d "slices" of a long cylindrical device. This is a method of getting an electric current source term that is large and entirely described by classical transport.

It is also possible to interpret the volumetric radial current source as being produced by a wave-particle interaction. In this picture, the wave is not modeled using the electromagnetic fields, due to its fast time scales, and only pushes a current. Its ponderomotive force might appear as a momentum source term.

Another interpretation to the current source might be an externally imposed shift in the magnetic field, which carries with it the electron fluid before friction is able to diffuse the field back.

APPENDIX B: RESOLVING RADIAL CURRENT IN A 1D MAGNETO-HYDRODYNAMIC MULTIPLE FLUID SIMULATION

The equations solved in MITNS, (1) and (2), are "MHD-like." Fast time scales are discarded, such as the electric field term in Ampère's law, in addition to the electron density and inertia terms.

Without the time derivatives in the electron continuity and momentum equations, the electron fluid density and velocity are evaluated algebraically from quasi-neutrality,

$$n_e = \sum_{s \neq e} Z_s n_s, \qquad (B1)$$

and form Ampère's law,

$$\mu_0 e n_e \mathbf{v}_e = \mu_0 \sum_{s \neq e} Z_s e n_s \mathbf{v}_s - \nabla \times \mathbf{B}. \qquad (B2)$$

Quasi-neutrality makes Gauss law inapplicable for a nonzero electric field. Instead, the electric field is determined from the inertia-less and nonviscous electron momentum equations. This electric field is also used to evolve the magnetic field.

MITNS has a one-dimensional domain, which restricts the allowed variations to the radial direction, If $\frac{\partial}{\partial \theta} = \frac{\partial}{\partial z} = 0$,

$$\nabla \times \mathbf{B} \cdot \hat{r} \equiv 0, \qquad (B3)$$

and no current can flow in the radial direction.

In order to explore radial plasma conductivity in this framework, that is, to look at the relation between j_r and the other physical quantities in the system, we must ignore Eq. (B3), and instead implement a current on the entire domain, similarly to a body force (such as gravity),

$$v_{er} = \left[\sum_{s \neq e} Z_s e n_s\right]^{-1} \cdot \left[\sum_{s \neq e} Z_s e n_s v_{sr} - j_r(r, t)\right]. \qquad (B4)$$

The function $j_r(r, t)$ has to be specified either as a local Ohm's law, or as an *a priori* driving force.

The algebraic nature of the MHD-like electric field prevents an application of boundary conditions to the electron momentum equation or to the electric field.

Azimuthal current can be injected into the simulated domain by applying a boundary condition to the magnetic field.

This solution adds to the electron velocity perpendicularly to the magnetic field. This does not represents a cross field transport of the electrons, as the magnetic field would be advected by the moving electron fluid. Adding the current to the electrons is numerically simple, and its effects are automatically implemented in the friction terms and magnetic field evolution. It also avoids changing

the accurate ion momentum equations. Attempting to add the imposed current to the ion velocities would require some partition of the current among an arbitrary number of ion fluids.

It is possible to evaluate, in post processing, the departure from quasi-neutrality using Gauss law by taking the divergence of the electric field calculated using Ohm's law. The current relates to the displacement current by

$$\nabla \cdot \mathbf{j} = -\varepsilon_0 \frac{\partial}{\partial t} \nabla \cdot \mathbf{E}, \tag{B5}$$

$$j_r = \frac{r_i j_r(r_i)}{r} - \varepsilon_0 \frac{\partial}{\partial t}\left(E_r - \frac{r_i E_r(r_i)}{r}\right), \tag{B6}$$

which would be a small, of $\mathcal{O}(v_A^2/c^2)$, with v_A being the Alfvén speed and c the speed of light.

REFERENCES

[1] R. F. Post, Nucl. Fusion **27**, 1579 (1987).

[2] R. Gueroult and N. J. Fisch, Phys. Plasmas **19**, 112105 (2012).

[3] A. I. Velikovich and J. Davis, Phys. Plasmas **2**, 4513 (1995).

[4] P. F. Knapp, M. R. Gomez, S. B. Hansen, M. E. Glinsky, C. A. Jennings, S. A. Slutz, E. C. Harding, K. D. Hahn, M. R. Weis, M. Evans, M. R. Martin, A. J. Harvey-Thompson, M. Geissel, I. C. Smith, D. E. Ruiz, K. J. Peterson, B. M. Jones, J. Schwarz, G. A. Rochau, D. B. Sinars, R. D. McBride, and P.-A. Gourdain, Phys. Plasmas **26**, 012704 (2019).

[5] M. R. Gomez, S. A. Slutz, P. F. Knapp, K. D. Hahn, M. R. Weis, E. C. Harding, M. Geissel, J. R. Fein, M. E. Glinsky, S. B. Hansen, A. J. Harvey-Thompson, C. A. Jennings, I. C. Smith, D. Woodbury, D. J. Ampleford, T. J. Awe, G. A. Chandler, M. H. Hess, D. C. Lamppa, C. E. Myers, C. L. Ruiz, A. B. Sefkow, J. Schwarz, D. A. Yager-Elorriaga, B. Jones, J. L. Porter, K. J. Peterson, R. D. McBride, G. A. Rochau, and D. B. Sinars, IEEE Trans. Plasma Sci. **47**, 2081 (2019).

[6] S. A. Slutz and R. A. Vesey, Phys. Rev. Lett. **108**, 025003 (2012).

[7] M. R. Gomez, S. A. Slutz, A. B. Sefkow, D. B. Sinars, K. D. Hahn, S. B. Hansen, E. C. Harding, P. F. Knapp, P. F. Schmit, C. A. Jennings, T. J. Awe, M. Geissel, D. C. Rovang, G. A. Chandler, G. W. Cooper, M. E. Cuneo, A. J. Harvey-Thompson, M. C. Herrmann, M. H. Hess, O. Johns, D. C. Lamppa, M. R. Martin, R. D. McBride, K. J. Peterson, J. L. Porter, G. K. Robertson, G. A. Rochau, C. L. Ruiz, M. E. Savage, I. C. Smith, W. A. Stygar, and R. A. Vesey, Phys. Rev. Lett. **113**, 155003 (2014).

[8] A. Bekhtenev, V. Volosov, V. Pal'Chikov, M. Pekker, and Y. N. Yudin, Nucl. Fusion **20**, 579 (1980).

[9] R. F. Ellis, A. B. Hassam, S. Messer, and B. R. Osborn, Phys. Plasmas **8**, 2057 (2001).

[10] A. J. Fetterman and N. J. Fisch, Phys. Rev. Lett. **101**, 205003 (2008).

[11] E. J. Kolmes, I. E. Ochs, and N. J. Fisch, Phys. Plasmas **25**, 032508 (2018).

[12] J.-M. Rax, R. Gueroult, and N. J. Fisch, Phys. Plasmas **24**, 032504 (2017).

[13] B. Bonnevier, Ark. Fys. **33**, 255 (1966), see https://www.osti.gov/biblio/4460205.

[14] B. Lehnert, Nucl. Fusion **11**, 485 (1971).

[15] T. Hellsten, Nucl. Instrum. Methods **145**, 425 (1977).

[16] M. Krishnan, Phys. Fluids **26**, 2676 (1983).

[17] M. Geva, M. Krishnan, and J. L. Hirshfield, J. Appl. Phys. **56**, 1398 (1984).

[18] D. A. Dolgolenko and Y. A. Muromkin, Phys.-Usp. **60**, 994 (2017).

[19] I. E. Ochs, R. Gueroult, N. J. Fisch, and S. J. Zweben, Phys. Plasmas **24**, 043503 (2017).

[20] V. B. Yuferov, S. V. Katrechko, V. O. Ilichova, S. V. Shariy, A. S. Svichkar, M. O. Shvets, E. V. Mufel, and A. G. Bobrov, Probl. At. Sci. Technol. **113**, 118 (2018), see https://vant.kipt.kharkov.ua/ARTICLE/VANT_2018_1/article_2018_1_118.pdf.

[21] R. Gueroult, J.-M. Rax, S. J. Zweben, and N. J. Fisch, Plasma Phys. Controlled Fusion **60**, 014018 (2018).

[22] A. J. Fetterman and N. J. Fisch, Phys. Plasmas **18**, 094503 (2011).

[23] T. Ohkawa and R. L. Miller, Phys. Plasmas **9**, 5116 (2002).

[24] T. M. O'Neil, Phys. Fluids **24**, 1447 (1981).

[25] J.-M. Rax and R. Gueroult, J. Plasma Phys. **82**, 595820504 (2016).

[26] R. Gueroult, J.-M. Rax, and N. J. Fisch, J. Clean. Prod. **182**, 1060 (2018).

[27] S. I. Braginskii, "Transport processes in a plasma," in *Reviews of Plasma Physics*, edited by M. A. Leontovich (Consultants Bureau, New York, 1965), Vol. 1, p. 205.

[28] V. M. Zhdanov, Plasma Phys. Controlled Fusion **44**, 2283 (2002).

[29] E. Litvinova Mitra, E. Kolmes, I. Ochs, M. Mlodik, T. Rubin, and N. Fisch, Phys. Lett. A **398**, 127284 (2021).

[30] E. J. Kolmes, I. E. Ochs, M. E. Mlodik, J.-M. Rax, R. Gueroult, and N. J. Fisch, Phys. Plasmas **26**, 082309 (2019).

[31] M. E. Mlodik, E. J. Kolmes, I. E. Ochs, and N. J. Fisch, Phys. Plasmas **28**, 052702 (2021).

[32] E. J. Kolmes, I. E. Ochs, M. E. Mlodik, and N. J. Fisch, Phys. Rev. E **104**, 015209 (2021).

[33] M. E. Mlodik, E. J. Kolmes, I. E. Ochs, and N. J. Fisch, Phys. Rev. E **102**, 013212 (2020).

[34] P. Ricci, F. Halpern, S. Jolliet, J. Loizu, A. Mosetto, A. Fasoli, I. Furno, and C. Theiler, Plasma Phys. Controlled Fusion **54**, 124047 (2012).

[35] J. Leake, C. DeVore, J. Thayer, A. Burns, G. Crowley, H. Gilbert, J. Huba, J. Krall, M. Linton, V. Lukin *et al.*, Space Sci. Rev. **184**, 107 (2014).

[36] A. A. Laguna, A. Lani, H. Deconinck, N. Mansour, and S. Poedts, J. Comput. Phys. **318**, 252 (2016).

[37] T. Rognlien, P. Brown, R. Campbell, T. Kaiser, D. Knoll, P. McHugh, G. Porter, M. Rensink, and G. Smith, Contrib. Plasma Phys. **34**, 362 (1994).

[38] R. Simonini, G. Corrigan, G. Radford, J. Spence, and A. Taroni, Contrib. Plasma Phys. **34**, 368 (1994).

[39] G. Radford, A. Chankin, G. Corrigan, R. Simonini, J. Spence, and A. Taroni, Contrib. Plasma Phys. **36**, 187 (1996).

[40] B. Braams, Contrib. Plasma Phys. **36**, 276 (1996).

[41] S. Wiesen, D. Reiter, V. Kotov, M. Baelmans, W. Dekeyser, A. Kukushkin, S. Lisgo, R. Pitts, V. Rozhansky, G. Saibene *et al.*, J. Nucl. Mater. **463**, 480 (2015).

[42] T. Rognlien, M. Rensink, and D. Stotler, Fusion Eng. Des. **135**, 380 (2018).

[43] P. Rambo and J. Denavit, Phys. Plasmas **1**, 4050 (1994).

[44] P. Rambo and R. Procassini, Phys. Plasmas **2**, 3130 (1995).

[45] D. Ghosh, T. D. Chapman, R. L. Berger, A. Dimits, and J. Banks, Comput. Fluids **186**, 38 (2019).

[46] E. Kolmes, I. Ochs, and N. Fisch, Comput. Phys. Commun. **258**, 107511 (2021).

[47] K. G. Whitney, Phys. Plasmas **6**, 816 (1999).

[48] D. S. Miller, Comput. Fluids **210**, 104672 (2020).

[49] B. van Leer, J. Comput. Phys. **32**, 101 (1979).